Ultrafast Charge Transfer in Amino-Substituted Boron Dipyrromethene Dyes and Its Inhibition by Cation Complexation: A New Design Concept for Highly Sensitive Fluorescent Probes

Matthias Kollmannsberger,[†] Knut Rurack,*[,‡] Ute Resch-Genger,[§] and Jörg Daub*[,†]

Institut für Organische Chemie der Universität Regensburg, D-93040 Regensburg, Germany, Institut für Physikalische und Theoretische Chemie, Humboldt Universität zu Berlin, Bunsenstrasse 1, D-10117 Berlin, Germany, and Bundesanstalt für Materialforschung und -prüfung (BAM), Rudower Chaussee 5, D-12489 Berlin, Germany

Received: June 22, 1998; In Final Form: September 23, 1998

The photophysical behavior of a newly synthesized aza crown-substituted boron−dipyrromethene (BDP) dye and its dimethylamino analogue were investigated with steady-state and time-resolved fluorometry and compared to a reference compound. In solvents more polar than hexane, excitation of the dyes leads to a fast charge transfer from the locally excited (LE) state to a weakly emissive charge-transfer (CT) state. The donor-substituted compounds show dual emission from the LE and CT state, both fluorescence quantum yields being low. The rate constant of excited-state charge separation, calculated from the global analysis of time-resolved emission data, was determined to 1.6×10^{11} s^{-1} in 1,4-dioxane. The crowned compound forms 1:1-complexes with various alkali and alkaline-earth metal ions, which exist as two conformers in solution. In these complexes, coordination of the cation to the nitrogen donor atom of the crown inhibits the charge-transfer process, leading to a cation-dependent enhancement of the LE emission and the fluorescence lifetimes by factors $>10^3$. This efficient "switching on" of the fluorescence renders the crowned BDP dye an extremely sensitive fluorescent probe for metal ions.

Introduction

The use of fluorescent sensor molecules for the detection of metal ions, organic, and biological analytes[1,2,3] has focused much research interest on the synthesis as well as the understanding of the photophysical mechanisms governing the spectroscopic behavior of such systems.[4−12] These fluorescent probes are either constructed as fluorophore−spacer−receptor or as intrinsic fluorescent probes.[13] In the former case fluorophore and receptor are separated by a short alkyl spacer, whereas in the latter case the receptor is part of the chromophore π-electron system. Here, the receptor usually acts as an electron-donating and the basic fluorophore as an electron-accepting moiety. For both types of fluorescent probes, nitrogen-containing crown ethers are often used as receptors, especially for metal ion recognition.

The optical properties of the intrinsically donor−acceptor-substituted fluoroionophores (ICT probes) are determined by a strong solvent-dependent behavior, and the fluorescence observed under many analytic conditions, i.e., in polar liquid media, is largely Stokes-shifted. In fluorophore−spacer−receptor systems, electronic interaction is only possible via long-range forces such as photoinduced electron transfer (PET). Binding of the analyte to the receptor decreases its electron-donating ability and thus leads to the inhibition of the quenching process(es) resulting in the "switching on/off" of the fluorescence; however, no spectral changes occur. In contrast, coordination to the nitrogen donor atom of the receptor of an intrinsic fluoroionophore not only leads to changes in fluorescence intensity and lifetime but provides additional information via spectral shifts in both absorption and emission. Whereas the latter effect is advantageous in terms of spectral discrimination of analytically relevant species, the fluorescence of these intrinsic probes is either quenched by cation complexation or the fluorescence enhancement factors (FEF) are comparatively small (factors of ca. 2−5). Systems showing large complexation-induced FEF, which are highly desirable in terms of low detection limits and high signal-to-noise ratios, are rare, and FEF between 30 and ca. 500 have been so far only reported for some fluorophore−spacer−receptor PET systems.[6,8,13]

During the last years, molecules consisting of aromatic amine donor groups directly and covalently bound to fluorophores such as anthracene,[14−20] pyrene,[20,21] phenanthrene,[22] or acridine/ium[5,23] have been studied extensively to elucidate the mechanism of the charge-transfer (CT) process that takes place upon excitation of the fluorophore. In polar solvents, emission occurs no longer from the locally excited (LE) state of the fluorophore but from a highly polar CT state that is either directly accessible via absorption or is formed in the picosecond time range after excitation. However, the exact mechanism of this process is still not fully understood, and different intramolecular reaction pathways during the lifetime of the excited state (e.g., the twisted intramolecular charge-transfer "TICT" model[24,25]) are discussed for these molecules. In some systems, charge transfer can be sufficiently described with a simple three-state model (e.g., *p*-phenanthryl dimethylaniline[22]). However, a nonexponential fluorescence decay behavior is observed for others (e.g., *p*-anthracenyl−dimethylaniline, ADMA[15−17,20]) suggesting a more complex situation involving different transient species. In contrast, in H-acidic solvents, protonation of the amino group

[†] Institut für Organische Chemie.
[‡] Institut für Physikalische und Theoretische Chemie.
[§] Bundesanstalt für Materialforschung und -prüfung.

10.1021/jp982701c CCC: $15.00
Published on Web 11/21/1998

blocks the charge-transfer process and reestablishes emission from the locally excited state as the major deactivation route.[13,26,27]

Recently, we have shown that the use of difluorobordiaza-*s*-indacenes (boron−dipyrromethene dyes, BDPs) as acceptor moieties and fluorophores in such systems yields highly sensitive fluorescent probes.[28−30] BDP dyes combine the advantages of high molar extinction coefficients (ϵ > 70 000 M^{-1} cm^{-1}) and high fluorescence quantum yields (ϕ_f ca. 0.5−0.8) and can be excited at relatively long wavelengths (ca. 500 nm). They are currently in use as laser dyes and fluorescent labels for biomolecules[31] and have been incorporated in an electron-transfer probe of radical ion pair generated electric fields.[32] The spectroscopically advantageous properties and the high electron affinity of the BDP fluorophore which promises fast and efficient charge transfer, led us to synthesize and investigate the crown ether analogue **1** of the dimethylanilino-substituted BDP dye **2** under the premise of developing new and highly sensitive fluorescent probes for metal ions. Here, for a better understanding of the operative fluorescence mechanisms, the photophysical properties of **1**, **2**, and the reference compound **3** are investigated by steady-state absorption and emission spectroscopy as well as time-resolved fluorometry in different solvents. Furthermore, the complexation of **1** with various alkali and alkaline-earth metal ions is spectroscopically studied and discussed.

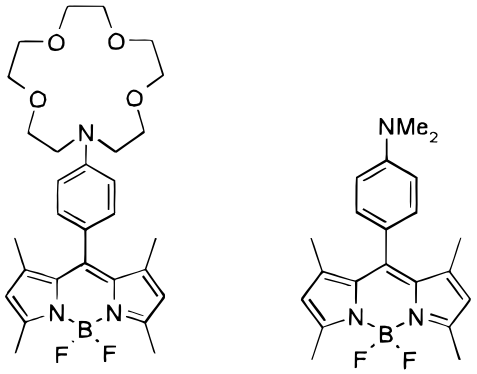

1 **2**

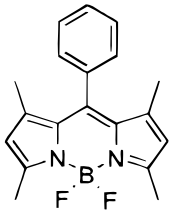

3

Experimental Section

Materials. Metal perchlorates purchased from Merck, Acros, and Aldrich were of highest purity available and dried in a vacuum oven before use.[33] All the solvents employed were of spectrometric grade. For the determination of the complex stability constants, acetonitrile was distilled from CaH_2 prior to use.

Apparatus. Melting points (uncorrected) were measured on a Kofler hot plate. IR spectra were obtained on a BioRad FTS 155 spectrometer. ^1H NMR spectra were recorded on a Bruker AC250 spectrometer.

Steady-State Spectroscopy. UV/vis spectra were obtained on a Perkin-Elmer Lambda9 UV/vis/NIR spectrophotometer and a Specord M400/M500 absorption spectrometer from Carl Zeiss. Steady-state emission spectra were recorded on a Hitachi F-4500 and a Spectronics Instruments 8100 spectrofluorometer. For the fluorescence experiments, only dilute solutions with an optical density (o.d.) below 0.01 at the excitation wavelength (o.d. < 0.04 at the absorption maximum) were used. For the determination of the relative fluorescence quantum yields (ϕ_f), the optical densities of the solutions at the excitation wavelengths were adjusted to an optical density of 0.1 ± 0.001 in a 100 mm absorption cell. These solutions were then transferred to a 10 mm quartz cell, and the fluorescence measurements were performed with a 90° standard geometry and an emission polarizer set at 54.7°. Fluorescein 27 in 0.1 N NaOH (ϕ_f 0.90 ± 0.03) and DCM in methanol (ϕ_f 0.43 ± 0.08) were used as fluorescence standards.[34] All the fluorescence spectra presented here are corrected for the spectral response of the detection system (calibrated quartz halogen lamp placed inside an integrating sphere; Gigahertz-Optik) and for the spectral irradiance of the excitation channel (calibrated silicon diode mounted at a sphere port; Gigahertz-Optik). The fluorescence quantum yields were calculated from multiple measurements (N = 6), and the uncertainties of the measurement were determined to ±5% (for 1.0 > ϕ_f > 0.2), ±10% (for 0.2 > ϕ_f > 0.02), ±20% (for 0.02 > ϕ_f > 5 × 10^{-3}), and ±30% (for 5 × 10^{-3} > ϕ_f), respectively.

Time-Resolved Spectroscopy. Fluorescence lifetime (τ_f) measurements were performed with a unique laser impulse fluorometer with picosecond time resolution described elsewhere.[35] The sample was excited with the second harmonic output (LBO crystal) of a regenerative mode-locked argon ion laser-pumped Ti:sapphire laser at a repetition rate of either 82 or 4 MHz (reduction by synchronized pulse selection). The emitted fluorescence was collected at right angles (polarizer set at 54.7°; monochromator with spectral bandwidths of 4, 8, and 16 nm), and the fluorescence lifetime profiles were recorded with a time-correlated single photon counting setup and a time division of 5.2 ps chn^{-1} (82 MHz version) and 52.6 ps chn^{-1} (4 MHz version) yielding the corresponding experimental accuracies of ±3 ps (82 MHz version) and ±0.04 ns (4 MHz version), respectively. The temporal response of the system was 35 ps, and the calibration of the experimental setup was checked with pinacyanol in ethanol (τ_f = 13 ± 1 ps),[36] rose bengal in methanol (τ_f = 0.50 ± 0.02 ns),[37] and fluorescein 27 in 0.1 N NaOH (τ_f = 4.50 ± 0.03 ns).[38] For the estimation of the color shift (wavelength-dependent temporal response of the detection system) between the instrumental response function and the actual fluorescence decay, the fluorescence of fluorescein 27 (in 0.1 N NaOH) and DCM (in ethanol) were quenched by saturation with potassium iodide, and their decay profiles were recorded at the corresponding emission wavelengths. Analysis of the fluorescence decay data was performed with a PC using the software packages IBH Decay Analysis Software V4.2 (IBH Consultants Ltd.) and Globals Unlimited V2.2 Time Domain (Globals Unlimited). The goodness of the fit of the single decays, as judged by reduced chi-squared (χ^2_R), the autocorrelation function $C(j)$ of the residuals, and the Durbin Watson parameter (DW), was always acceptable yielding values of χ^2_R < 1.2 and DW > 1.8. In the case of the global analysis of the decays recorded at different emission wavelengths, the decay times of the species are linked while the program varies the preexponential factors and time constants until the changes in the error surface (χ^2 surface) are minimal, i.e., convergence

is reached. The fitting results are judged for every single decay (local χ^2_R) and for all the decays (global χ^2_R). The errors for all the measurements presented here were below global $\chi^2_R = 1.2$.

The rate constants of radiative k_f and nonradiative k_{nr} deactivation were generally calculated from the measured fluorescence quantum yields and fluorescence lifetimes according to eqs 1 and 2; other equations used to calculate rate constants of reactions in the excited state are given in the corresponding paragraphs.

$$k_f = \frac{\phi_f}{\tau_f} \quad (1)$$

$$k_{nr} = \frac{(1 - \phi_f)}{\tau_f} \quad (2)$$

Complex Stability Constants. The complex stability constants K were measured by titrating 10^{-6} M solutions of **1** in acetonitrile with stock solutions of metal perchlorates and monitoring the changes in fluorescence. From a least-squares analysis of a plot according to eq 3, K can be determined from the slope; the reported values are mean values of at least two measurements with correlation coefficients >0.99.

$$\frac{I_f - I_0}{I_{max} - I_r} = K[M] \quad (3)$$

The values of K, measured at two different excitation (480 and 495 nm) and detection (505 and 510 nm) wavelengths, are in good agreement.

Syntheses. Compounds **1**−**3** were prepared from 2,4-dimethylpyrrole[39] and *p*-formylphenylaza-15-crown-5[40] (**1**), *p*-dimethylaminobenzaldehyde (**2**), and benzaldehyde (**3**) in a one-pot reaction. General procedure: 4 mmol of 2,4-dimethylpyrrole and 2 mmol of the aldehyde were dissolved in 250 mL of absolute methylene chloride under nitrogen atmosphere. One drop of trifluoroacetic acid was added and the solution stirred at room temperature until TLC-control (silica; **1**, ethyl acetate; **2**, **3**, CH_2Cl_2) showed complete consumption of the aldehyde. At this point, a solution of 2 mmol dichlorodicyanobenzoquinone (DDQ) in CH_2Cl_2 was added, and stirring was continued for 15 min followed by addition of 4 mL of *N*-ethyl-*N*,*N*-diisopropylamine and 4 mL of $BF3{\cdot}Et_2O$. After stirring for another 30 min the reaction mixture was washed with water and dried, and the solvent was evaporated. The residue was chromatographed twice on a silica column (**1**, ethyl acetate/methanol 10:1, second chromatography CH_2Cl_2/MeOH 20:1; **2**, **3**, CH_2Cl_2). Recrystallization from ethyl acetate/hexane (**1**) or $CHCl_3$/hexane (**2**, **3**) yielded analytically pure samples.

1: Yield: 758 mg (1.40 mmol, 70%). Red crystals, mp 178−179 °C. IR (KBr): 1545, 1509 (C═C, C═N), 1198 (B−F). ^{1}H NMR ($CDCl_3$): 1.50 (s, 6H, CH_3), 2.54 (s, 6H, CH_3), 3.61−3.71 (m, 16H, crown), 3.77−3.82 (m, 4H, crown), 5.97 (s, 2H,), 6.7−7.1 (m, 4H, phenyl). MS (EI, 70 eV): *m*/*z* (%) 541.4 (100%, $M^{\bullet+}$). Calculated for $C_{29}H_{38}N_3O_4BF_2$: C 64.34, H 7.07, N 7.76. Found: C 64.37, H 7.07, N 7.62.

2: Yield: 270 mg (0.74 mmol, 37%). Orange needles, mp 227 °C. IR (KBr): 1542, 1509 (C═C, C═N), 1196 (B−F). ^{1}H NMR ($CDCl_3$): 1.49 (s, 6H, CH_3), 2.55 (s, 6H, CH_3), 3.02 (s, 6H, $N(CH_3)_2$), 5.96 (s, 2H), 6.77 (m, 2H, phenyl), 7.08 (m, 2H, phenyl). MS (EI, 70 eV): 367 (100%, $M^{\bullet+}$), 352 (24%, $M - CH_3^{\bullet+}$), 347 (34%), ($M - HF^{\bullet+}$). Calculated for $C_{21}H_{24}N_3BF_2$: C 68.68, H 6.59, N 11.45. Found: C 68.53, H 6.66, N 11.43.

3: Yield: 280 mg (0.86 mmol, 43%). Green crystals, mp 172−175 °C. IR (KBr): 1544, 1510 (C═C, C═N), 1190 (B−F); ^{1}H NMR ($CDCl_3$): 1.37 (s, 6H, CH3), 2.56 (s, 6H, CH3), 5.98 (s, 2H,), 7.26−7.30 (m, 2H, phenyl), 7.47−7.50 (m, 3H, phenyl). MS (EI, 70 eV): 324 (100%, $M^{\bullet+}$), 309 (65%, $M - CH_3^{\bullet+}$), 304 (67%, $M - HF^{\bullet+}$). Calculated for $C_{19}H_{19}N_2BF_2$: C 70.41, H 5.87, N 8.65. Found: C 70.33, H 5.93, N 8.64.

Results and Discussion

Absorption and Emission of 1, 2, and 3 in Different Solvents. **1**, **2**, and **3** show identical absorption spectra with an absorption pattern typical for BDP chromophores.[41] In hexane, a strong S_0-S_1 transition with a maximum at 500 nm ($\epsilon = 88\,000$ M^{-1} cm^{-1}) and a shoulder at the shorter wavelength side as well as a broader, much weaker transition at 380 nm ($\epsilon = 6000$ M^{-1} cm^{-1}) are observed. No long wavelength CT absorption is present in **1** and **2**. The similar absorption spectra of **1**, **2**, and **3** indicate the absence of donor−acceptor interactions in the ground state, which is obviously due to the sterically demanding methyl groups that force the molecule into a twisted conformation. An X-ray structure of a similar compound showed the twist angle between the phenyl ring and the BDP chromophore to be 75°.[28] Furthermore, the absorption spectra are only barely affected by solvent polarity, the maximum being slightly shifted hypsochromically (ca. 5 nm) with increasing polarity for **1**−**3**. (Table 1).

Unlike their absorption properties, the emission behavior of **1** and **2** is strongly solvent-dependent (Figure 1). In hexane, **1** and **2** show emission from the locally excited state of the BDP fluorophore at 508 nm shaped like a mirror image of the absorption spectrum. Similar effects occur for the reference compound **3**. In more polar solvents, this emission is strongly quenched; in diethyl ether by factors of 65 (**1**) and 25 (**2**) and in acetonitrile by factors of 1.3×10^3 (**1**) and 1×10^3 (**2**), respectively. Along with the decrease in LE emission, the formation of a second broad emission band is observed at longer wavelengths showing rather low fluorescence quantum yields and a strongly solvatochromic behavior (Table 1 and Figure 1). The fluorescence quantum yields of the two emission bands of **1** and **2** in diethyl ether, 1,4-dioxane, and tetrahydrofuran were calculated after spectral separation. The LE band was modeled by fitting the emission spectrum of **3** in the corresponding solvent to two log-normal functions describing the sub and the main band centered at 530 and 508 nm. In a fit of the spectra showing dual emission, the position, half-width, and skewness of these two components were kept fixed (within a certain interval) and a third log-normal function was included to describe the remaining long wavelength band. An example of a fit is given in Figure 2, and the calculated fluorescence quantum yields are included in Table 1.

The intensity of the long wavelength emission band decreases with increasing solvent polarity, and the center of the band shifts to the red; in acetonitrile, it could not be detected at all. Fluorescence excitation spectra of **1** and **2** recorded with the detection wavelength set in both regions, i.e., the LE as well as the long wavelength emission band, have identical shapes and match the UV/vis absorption spectra. This indicates that the long wavelength emission originates from a species formed after excitation of the BDP chromophore and both the solvatochromism and the positive solvatokinetic effect suggest a highly dipolar nature. We attribute this red emission to a species having pronounced charge-transfer (CT) character similar to that in *p*-anthracenyl dimethylaniline and related compounds, which is formed by a fast reaction in the excited state.

TABLE 1: Absorption and Emission Properties of 1, 2, and 3 in Different Solvents[61]

	λ_{abs}/nm	λ_{em} (LE)/nm	λ_{em} (CT)/nm	Φ_f (LE)	Φ_f (CT)	Φ_f (CT)/Φ_f (LE)	τ_1/ps	τ_3/ps	τ_2/ns	$k_f/10^9$ s^{-1}	$k_{nr}/10^9$ s^{-1}
					1						
hexane	500	508		0.26			1590			0.16	0.46
Et_2O	498	510	613	0.004	0.050	12	15	405	3.65		
dioxane	500	511	637	0.001	0.033	33	6	150	3.54		
THF	500	511	684	0.0003	0.014	47	<3	76	2.45		
MeCN	496	505	*a*	0.0002	*a*		5		2.56		
					2						
hexane	500	508		0.31			1610			0.19	0.43
Et_2O	498	509	615	0.012	0.050	4.2	10		3.54		
dioxane	500	510	645	0.004	0.029	7.2	6		3.50		
THF	500	512	706	0.001	0.009	9.0	4		2.40		
MeCN	496	505	*a*	0.0003	*a*		3		2.79		
					3						
hexane	500	510		0.50			2720			0.18	0.18
Et_2O	498	510		0.59			2980			0.20	0.14
dioxane	500	510		0.58			3350			0.17	0.12
THF	500	510		0.56			3060			0.18	0.14
MeCN	497	505		0.60			3170			0.19	0.13

[a] Too low to be measured

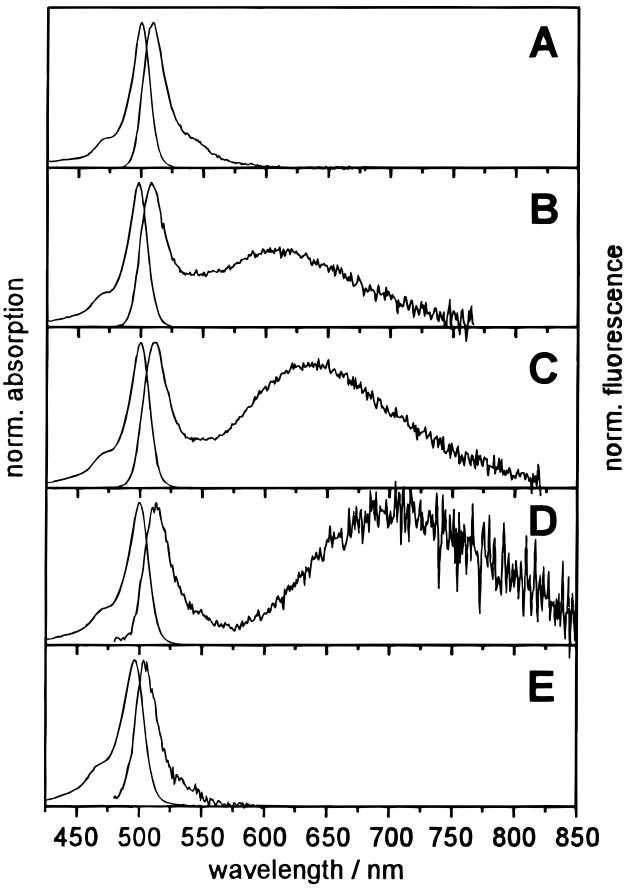

Figure 1. Absorption and emission spectra of **2** in hexane (A), diethyl ether (B), 1,4-dioxane (C), tetrahydrofuran (D), and acetonitrile (E). The spectra are normalized for better comparison (excitation at 475 nm).

The fluorescence decay profiles of the reference compound **3** could be described by a single-exponential fit (fluorescence lifetimes τ_f of 2.7−3.3 ns) in all the solvents investigated; in fact, the radiative rate constants of 0.18×10^9 s^{-1} are identical within experimental errors (Table 1). In hexane, the emission of **1** and **2** centered at 508 nm decays monoexponentially as well, yielding similar radiative rate constants. The nonradiative rate constants are slightly higher than for **3**, which may be attributed either to the higher conformational flexibility due to the attached dimethylamino and crown substituents or to the interaction with an energetically low-lying local triplet state (increase of k_{isc}).[42] In solvents more polar than hexane, the fluorescence decays of both **1** and **2** could be only fitted to the sum of at least two exponentials leading to lifetimes in the 3−10 ps (fast component) and the 2−3 ns (slow component) time range. Measurements of the fluorescence decay profiles as a function of emission wavelength in the region of 495−690 nm revealed a decrease of the relative amplitude of the fast component with increasing detection wavelength and the vice versa behavior of the relative amplitude of the slow component. This is consistent with a mechanism involving the excitation of a single ground-state species to a LE state followed by a fast reaction to a CT state (Scheme 1). Thus, the lifetime of the LE state is substantially shortened and its fluorescence decays with a high rate constant, whereas the slow component can be attributed to the CT state.

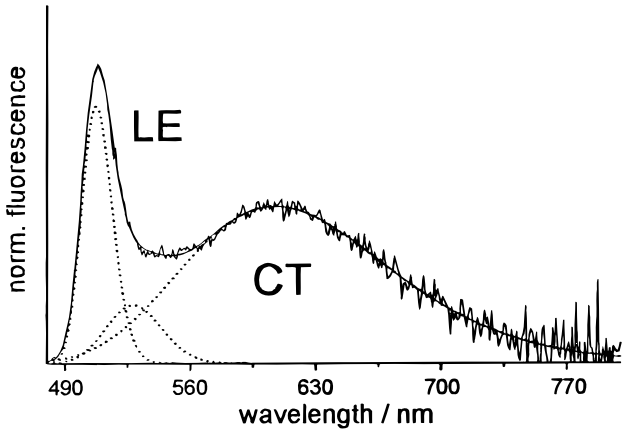

Figure 2. Fit of the LE and CT band of the emission spectrum of **2** in diethyl ether. The LE band is modeled from the main band and the subband of **3** in diethyl ether (full lines, measured spectrum and fit; dotted lines, single components; excitation at 475 nm).

Having this picture in mind, the occurrence of a rise time should be expected in the spectral region of the CT emission. This rise time should be similar to the main decay time of the LE band, i.e., the lifetime of the fast decay component, because owing to sterical restriction and fast charge transfer, a substantial contribution from other transient species seems to be rather unlikely. However, it is difficult to detect the rise times owing

SCHEME 1: Generalized Kinetic Scheme for the Photophysical Processes Governing the Excited-State Behavior of 1 and 2 Involving Two or Three Excited Species (LE, CT, (TS)) in Possible Parallel or Consecutive Reaction Mechanisms[a]

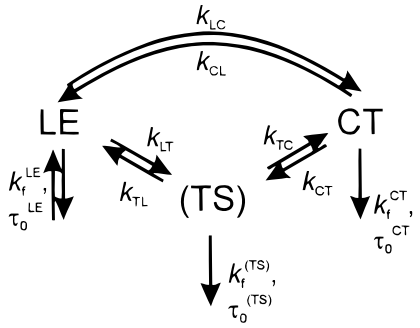

[a] For 2, only the LE and CT state are involved and thus $k_{LT} = k_{TL} = k_{TC} = k_{CT} = 0$; (TS) = transitional or third species.

to the large differences in the two lifetimes and the limitations of our experimental setup. We were at least able to detect these rise times for **1** and **2** in diethyl ether and for **2** in 1,4-dioxane, and, indeed, the rise times are very similar to the decay times of the fast component. In acetonitrile, the emission from the CT state is extremely weak, and therefore, the relative amplitude of the long-lived decay component is very small (<0.5%) making the determination of the rise time impossible.

Furthermore, for **1**, a third decay component with a relative amplitude of ≤0.05 and time constants of $\tau_3 = 405$ ps (diethyl ether), 150 ps (1,4-dioxane), and 76 ps (tetrahydrofuran) was observed in these three solvents. However, such a third decay component could not be detected for **2**. Obviously, a third, weakly fluorescing species with pronounced CT character is involved in the fluorescence behavior of **1**. This third decay component (TS) could be due to a double minimum in the potential surface of the excited CT state as a function of the twist angle between the donor and the acceptor, a mechanism recently observed in highly pretwisted biphenyls.[43] However, it was not possible to detect a second rise time, and the limiting experimental possibilities, especially in the NIR region, do not allow for a global analysis of the wavelength-dependent fluorescence decay data with respect to the verification of such an excited-state reaction mechanism.[44] Therefore, the real nature of this species and the deactivation process of the initially excited **1** (Scheme 1) remain unclear at present.

To determine the rate constants governing the excited-state reaction and relaxation processes in **2**, we performed a global analysis of the time- and wavelength-resolved emission data in diethyl ether and 1,4-dioxane. The temporal evolution of a fluorescence decay corresponding to a two-state model, i.e., emission from the LE and CT state, can be described by a sum of two exponentials:

$$I_{LE}(t) = A_{11}\, e^{-t(\tau_1)^{-1}} + A_{12}\, e^{-t(\tau_2)^{-1}} \quad (4)$$

$$I_{CT}(t) = A_{21}\, e^{-t(\tau_1)^{-1}} + A_{22}\, e^{-t(\tau_2)^{-1}} \quad (5)$$

The two decay rates τ_i^{-1} directly observed in the experiment are linked to the species-related fluorescence lifetimes τ_0^X ($X = LE$, CT) through eqs 6−9 involving the rate constants of the excited-state reactions, k_{LC} and k_{CL}.[45,46] Using the decay times τ_i and amplitudes A_{ij} given in the caption of Figure 3 and a reasonable estimate for τ_0^{LE}, an analytical solution of eqs 6−9 yields the photophysical parameters given in Table 2.[45−47]

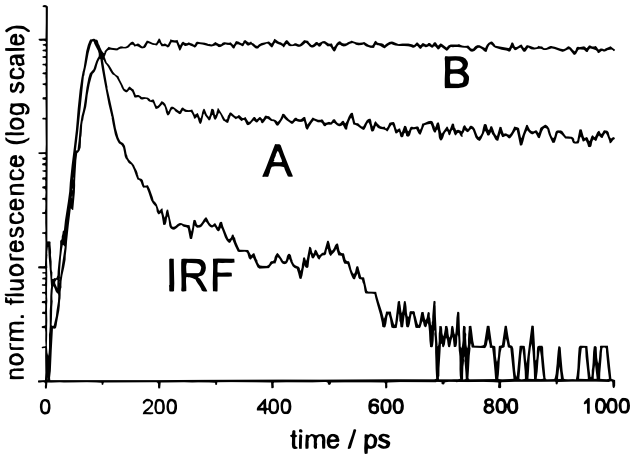

Figure 3. Normalized fluorescence decay curves of **2** in diethyl ether at 500 nm (curve A) and 670 nm (curve B); instrumental response function (IRF) shown for comparison. Global analysis with $\tau_1 = 3.42$ ns and $\tau_2 = 11$ps yields $A_{11} = 1.36$ and $A_{12} = 24.2$ for curve A and $A_{21} = 5.1$ and $A_{22} = -4.9$ for curve B, respectively (excitation at 475 nm).

TABLE 2: Calculated Photophysical Parameters of the Dimethylamino Compound 2

solvent	$k_{LC}/10^9\ s^{-1}$	$k_{CL}/10^9\ s^{-1}$	$(\tau_0^{CT})^{-1}/10^9\ s^{-1}$	k_f^{CT}/k_f^{LE}
diethyl ether[a]	85.8	4.8	0.29	0.234
1,4-dioxane[b]	163	2.9	0.32	0.132

[a] See Figure 3 for values of A_{ij}. [b] Global analysis with $\tau_1 = 3.09$ ns and $\tau_2 = 6$ ps yields $A_{11} = 1.32$ and $A_{12} = 73.8$ for a fluorescence decay monitored at 500 nm.

$$\frac{A_{12}}{A_{11}} = \frac{X - \tau_1^{-1}}{\tau_2^{-1} - X} \quad (6)$$

$$X = k_{LC} + (\tau_0^{LE})^{-1} \quad (7)$$

$$Y = k_{CL} + (\tau_0^{CT})^{-1} \quad (8)$$

$$\tau_{1,2}^{-1} = \frac{1}{2}\{(X + Y) \pm [(X - Y)^2 + 4k_{LC}k_{CL}]^{1/2}\} \quad (9)$$

The resulting rate constants for the formation of the CT state of $8.6 \times 10^{10}\ s^{-1}$ in diethyl ether and $1.6 \times 10^{11}\ s^{-1}$ in 1,4-dioxane document the ultrafast charge transfer that occurs after excitation of the BDP fluorophore. The high efficiency of this charge-transfer process in such solvents of medium polarity is also exemplified by the high ratio of k_{LC}/k_{CL} of 18 in diethyl ether and 56 in 1,4-dioxane.

Having Scheme 1, the kinetic parameters given in Table 2, and the efficient excited-state CT reaction in mind, construction of the decay as well as the species associated spectra ($DAS_i(\lambda)$ and $SAS_i(\lambda)$) allows for a verification of the kinetic model employed. The $DAS_i(\lambda)$ and $SAS_i(\lambda)$ are given by eqs 10−14.[48]

$$I_{tot}(\lambda, t) = \sum_i A_i(\lambda)\, e^{-t(\tau_i)^{-1}} \quad (10)$$

$$DAS_i(\lambda) = \frac{A_i(\lambda)\, F_{SS}^{tot}(\lambda)}{\sum_i A_i(\lambda)\tau_i} \quad (11)$$

$$SAS_i(\lambda) = F_{SS}^{tot}(\lambda)\int_0^\infty \frac{I_i}{I_{tot}}(\lambda, t)\,dt, \quad \text{with} \quad i = \text{LE} \quad \text{or} \quad \text{CT} \tag{12}$$

$$SAS_{LE}(\lambda) = [DAS_1(\lambda) + DAS_2(\lambda)]\tau_1\tau_2 Y \tag{13}$$

$$SAS_{CT}(\lambda) = [(\tau_2^{-1} - Y)DAS_1(\lambda) - (Y - \tau_1^{-1})DAS_2(\lambda)]\tau_1\tau_2 \tag{14}$$

where $I_{tot}(\lambda, t)$, $A_i(\lambda)$, and τ_i are the overall fluorescence intensity, the amplitudes, and corresponding fluorescence decay times of the species i from the time-resolved measurements and $F_{SS}^{tot}(\lambda)$ is the integral steady-state emission spectrum. Furthermore, assuming that in the high-energy region of the spectrum only the LE species emits, $SAS_{LE}(\lambda)$ can be substituted by $F_{SS}^{tot}(\lambda)$ in eq 13. In this (short or "blue" wavelength) spectral region where $I_{CT} \rightarrow 0$, convergence of a plot of $Y(\lambda)$ vs λ yields the true value of Y (for **2** in diethyl ether $Y(\lambda \rightarrow \lambda_{blue}) = 4.99 \times 10^9\ s^{-1}$).[49] When no backward reaction occurs, this value must equal the value for Y in an irreversible process, $Y^{irr} = \tau_1^{-1}$. With $\tau_1 = 3.42$ ns, as indicated in the caption of Figure 3, a value of $Y^{irr} = 2.93 \times 10^8\ s^{-1}$ is obtained, clearly smaller than that found in the experiment. This corroborates the fact that although the forward CT process is fast and efficient, the backward reaction is not negligible.

The rate constants for fluorescence deactivation of both emitting states can be compared when plotting the concentration ratio c_{CT}/c_{LE} as a function of time (see eq 15) and calculating k_f^{CT}/k_f^{LE} from the ratio of both the fluorescence intensities and concentrations of the species (LE and CT) at equilibrium ($t \rightarrow \infty$) according to eq 16.[50] In both solvents analyzed, this ratio is less than 1 (Table 2) pointing to a strongly forbidden transition in the CT state of **2**.

$$\frac{c_{CT}(t)}{c_{LE}(t)} = \frac{k_{LC}(e^{-t(\tau_1)^{-1}} - e^{-t(\tau_2)^{-1}})}{(\tau_2^{-1} - X)e^{-t(\tau_1)^{-1}} + (X - \tau_1^{-1})e^{-t(\tau_2)^{-1}}} \tag{15}$$

$$\frac{\Phi_{CT}}{\Phi_{LE}} = \frac{k_f^{CT}c_{CT}(t)}{k_f^{LE}c_{LE}(t)} = \frac{k_f^{CT}k_{LC}}{k_f^{LE}[k_{LC} + (\tau_0^{CT})^{-1}]} \tag{16}$$

The main driving force for the very fast formation of the highly polar, weakly emissive CT state is the high electron affinity of the BDP fluorophore documented by its reduction potential (−1.26 V vs SCE for **3**[28] compared to, e.g., −2.22 V vs SCE[51] for phenylanthracene). Similar fast charge-transfer reactions in the excited state have been observed in rhodamine[27] systems where the fluorophore is also very electron deficient (−0.8 to −0.9V vs SCE for several rhodamines[52]).

Because of the nearly perpendicular conformation of **1** and **2** in the CT state, the transition moment is very small and the radiative deactivation strongly forbidden, which results in small rate constants for fluorescence deactivation and a ratio of $k_f^{CT}/k_f^{LE} < 1$. A similar tendency has been reported for ADMA and its preorientated derivative 3,5-dimethyl-ADMA, which has a twist angle of ca. 65°.[14,16,17]

The charge-transfer process can be efficiently blocked by protonation. In acetonitrile, the effect of protonation on the absorption behavior of **1** and **2** is small and only a slight bathochromic shift can be observed. In contrast, the emission properties are drastically altered (Table 3). Independent of solvent, protonation turns **1** and **2** into highly fluorescent molecules: the CT emission disappears and the emission from the LE state with its characteristically high fluorescence quantum yield is reestablished. Time-resolved fluorescence measurements yield monoexponential decay kinetics, the lifetime of the LE state being increased by a factor of ca. 1000, and calculated radiative rate constants similar to that of the reference compound **3**.

TABLE 3: Protonation-Induced Changes in the Photophysical Properties of 1 and 2 in MeCN

	λ_{abs}/nm	λ_{em}/nm	Φ_f	τ (LE)/ps	$k_f/10^9\ s^{-1}$	$k_{nr}/10^9\ s^{-1}$
1	496	505	0.0002	5		
2	496	505	0.0003	2.6		
1-H^+	500	510	0.68	3800	0.179	0.084
2-H^+	500	510	0.49	2900	0.169	0.176
3	497	505	0.60	3170	0.19	0.13

Complexation Studies

Having the strong and analytically valuable proton-induced effects on the absorption and emission behavior of the amino-substituted BDP derivatives in mind, we examined the photophysical changes of **1** upon complexation to the alkali and alkaline-earth metal cations Li^+, Na^+, Mg^{2+}, Ca^{2+}, Sr^{2+}, and Ba^{2+} in acetonitrile in order to test its possible application as a fluorescent probe. The complexation-induced effects on the steady-state absorption and emission spectra are similar to those found in the protonation studies, i.e., only a small change in absorption (Table 4) but a strong increase in the BDP LE emission. Moreover, the fluorescence excitation spectra measured at different emission wavelengths always match and resemble the corresponding absorption spectra. No cation-dependent shifts of the emission band were detectable, which leads to the conclusion that binding of a cation to the crown ether moiety only suppresses the charge-transfer process owing to electrostatic interaction between the positively charged cation and the nitrogen electron donor atom. As can be deduced from the data in Table 4, complexation of the employed alkali and alkaline-earth metal ions leads to FEF whose size depend on both the charge density and the extent of coordination to the crown nitrogen (Figure 4). Analysis of the fluorescence titration curves according to eq 3 (see Experimental Section) shows that in all the cases studied complexes of a well-defined 1:1-stoichiometry were formed (Figure 5). The effect of complexation on the fluorescence quantum yields is very remarkable, i.e., the chelation-induced FEF vary from 90 for Li^+ to 2250 for Mg^{2+}. To the best of our knowledge, the FEF observed for the alkaline-earth metal ions are among the highest fluorescence enhancement values reported in the literature until today.

In contrast to the steady-state fluorescence measurements, which suggest a quite simple complexation behavior of **1**, fluorescence decay measurements reveal a more complex situation. The lifetime of the LE emission increases drastically upon complexation (Table 1/Table 4), but the fluorescence decay curves of all the metal ion complexes measured can be described only by a biexponential fit, with the exception of the Mg^{2+} complex. In all the cases studied, the relative amplitudes of the two distinct decay components are independent of excitation (for wavelengths <495 nm) and observation wavelength, and no rise times were found.

Recalling the circumstances for the appearance of two distinct fluorescence lifetimes, they can be caused either by a photo-induced process in the excited state (an intra- or an intermolecular photophysical reaction) or by simultaneous excitation of two different ground-state species. The absence of any shifts in the steady-state emission spectra and the lack of a rise time at the red edge of the emission band do not suggest the involvement of an excited-state reaction such as a charge-transfer

TABLE 4: Complex Formation and Photophysical Data of the Complexes of 1 with Alkali and Alkaline-Earth Metal Ions in MeCN (Cavity Size of the Aza Crown: 1.7−1.8 Å)[a]

	λ_{abs}/nm	λ_{em}/nm	cation size[b]/Å	charge density/Z^2 Å^{-1}	log K_{tot}	Φ_f	FEF	τ_1/ps	$A_1/(A_1+A_2)$	τ_2/ns	F_{SS}^1/F_{SS}^2
1-Li^+	498	508	1.52 (6)	1.32	2.55	0.018	90	45	0.38	0.54	0.05
1-Na^+	498	508	2.04 (6)	0.98	2.20	0.097	485	64	0.45	1.75	0.02
1-Mg^{2+}	498	508	1.44 (6)	5.55	2.90	0.45	2250			2.95	
1-Ca^{2+}	498	508	2.12 (7)	3.77	4.40	0.34	1700	1050	0.56	3.30	0.41
1-Sr^{2+}	498	508	2.52 (8)	3.17	3.34	0.25	1250	820	0.71	3.18	0.64
1-Ba^{2+}	498	508	2.94 (9)	2.72	3.10	0.12	600	430	0.86	2.75	0.92
1-H^+	500	510				0.68	3400			2.90	

[a] Value taken from ref 62. [b] Taken from ref 58; in brackets: coordination numbers of the cation, taken from ref 5c.

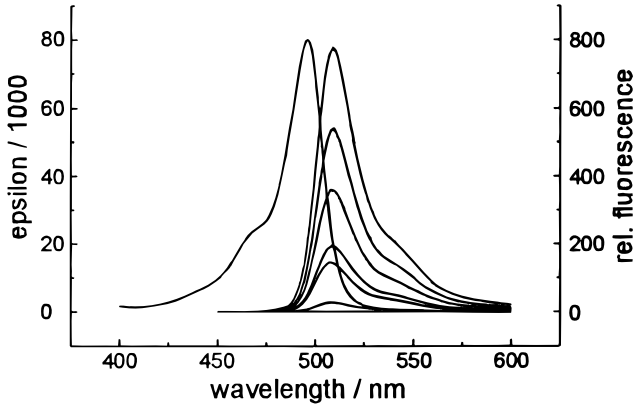

Figure 4. Absorption spectrum of **1** (left) and emission spectra of the complexes with (from top to bottom) Mg^{2+}, Ca^{2+}, Sr^{2+}, Ba^{2+}, Na^+, Li^+, and the free ligand in MeCN (excitation at 480 nm).

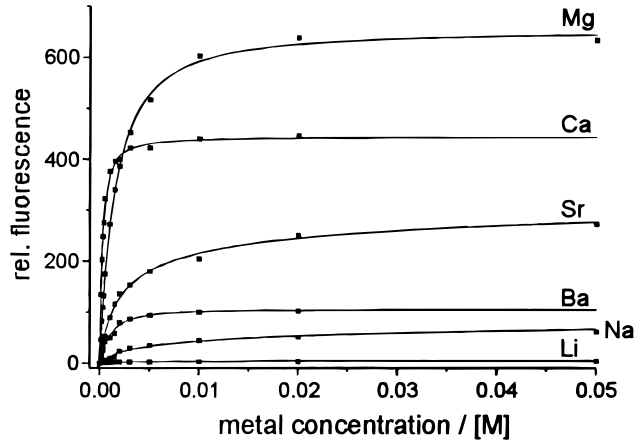

Figure 5. Changes in fluorescence intensity upon addition of metal ions (excitation at 480 nm, detection at 515 nm).

process or the photoinduced decoordination of the cation. The product of a charge-transfer reaction would have a more polar CT character, its emission should appear red-shifted compared to the precursor's, and a rise time would be expected. Especially in the case of the alkaline-earth metal cations showing two fluorescence decay times in the nanosecond time range with comparable relative amplitudes, such a rise time would have been detected by our instrumental setup. In case of photodecoordination of the cation,[4d,9c] the fluorescence lifetimes of the decoordinated complexes are similar for different cations, in sharp contrast to our measurements. These excited-state decoordination reactions are very fast (picosecond time scale), and emission is only observed from the decoordinated species; i.e., monoexponential decay kinetics are observed.[9c] On the other hand, the lack of any dependence of the fluorescence excitation spectra on the emission wavelength does not favor the existence of two different ground-state species at first sight. Yet, if two species have nearly the same absorption and emission spectra

TABLE 5: Fluorescence Decay Times of the Ba^{2+} Complex as a Function of Ion-to-ligand Ratio

ratio Ba^{2+}/1	τ_1/ps	$A_1/(A_1+A_2)$	τ_2/ns[a]
40:1	488	0.85	2.59
400:1	460	0.86	2.54
2250:1	424	0.85	2.52

[a] The value of τ_2 given in Table 5 is shorter compared to that given in Table 4. This is due to a different repetition rate (here: 82 MHz with a time window of 12 ns) used in these time-resolved experiments and the software-dependent neglect of the predecessor decay in the fits given in Table 5. The value obtained in the 4 MHz experiments (Table 4) is correct.

and only differ in their fluorescence quantum yields, it is very difficult to discriminate between them using steady-state measurements.

For a better understanding of this behavior, we performed time-resolved measurements with solutions containing **1** and Ba^{2+} in the ratios of 2250:1 (full complexation), 400:1, and 40:1 (Table 5). Again, these experiments revealed no dependence of the fluorescence lifetimes on the detection wavelength as well as no dependence of their relative amplitudes on the metal-to-ligand-ratios used.[53] This excludes the consecutive formation of two species with a 1:1 and a 1:2 stoichiometry and different complexation constants in a titration. The two species must be therefore formed simultaneously. The two decay times of the free ligand in the partly complexed solutions could not be detected here because of the very low emission of the ligand with respect to the complexes.

We tentatively attribute this behavior to the existence of two distinct conformers of the complexes in the ground state with very similar absorption and LE emission spectra but different fluorescence quantum yields and lifetimes.

This implies that that the fluorescence quantum yields obtained for the cation complexes are average values of the two conformers weighted by their relative concentrations c_r, except for the Mg^{2+} complex, which exists only in one stable ground-state conformation:

$$\Phi = c_{r1}\Phi_1 + c_{r2}\Phi_2 \qquad (17)$$

With eq 17 it is not possible to determine the ratio of the conformers, the individual Φ_i, and the corresponding radiative and nonradiative rate constants, but the contributions of both species to the overall fluorescence quantum yield can be derived from a global analysis of the wavelength-resolved fluorescence decay data.

Assuming that the equilibrium of conformers in the ground and in the excited state is the same and that any reaction in the excited state is slower than the involved relaxation processes, it is possible to construct the decay-associated spectra from the time-resolved fluorescence data according to eqs 10 and 11.[48] In the absence of any excited-state reaction, these $DAS_i(\lambda)$ values are identical with the SAS, i.e., the contribution F_{SS}^i of

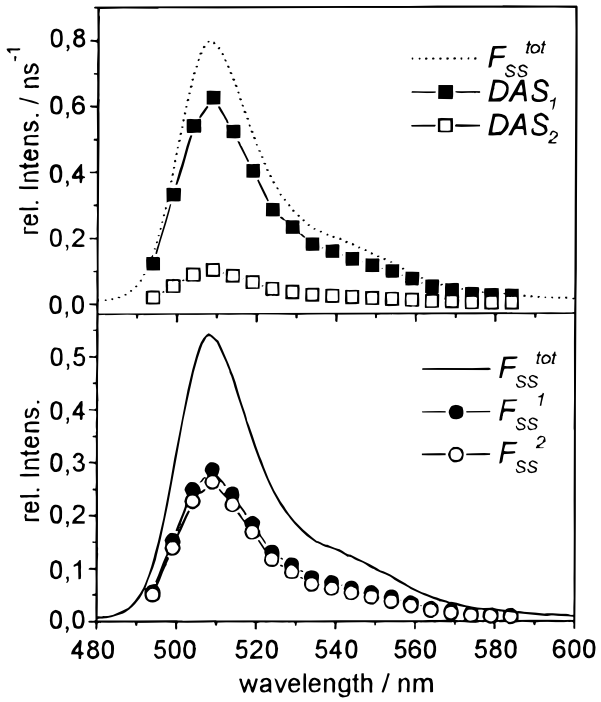

Figure 6. $DAS_i(\lambda)$ (upper part) and spectral contributions $F_{SS}{}^i$ (lower part) of the two decaying species of the Ba^{2+} complex at M:L = 400:1. The indices *1* and *2* correspond to the species decaying with τ_f = 460 ps (*1*) and τ_f = 2.54 ns (*2*). In the lower part, the full line represents the steady-state emission spectrum of the mixture, and the same spectrum (dotted line) is included in the upper part for better comparison (excitation at 485 nm, explanation see text).

the single species to the overall fluorescence intensity (see Table 4):

$$F_{SS}{}^i(\lambda) = \frac{DAS_i(\lambda)\tau_i^{-1} F_{SS}{}^{tot}(\lambda)}{\sum_i DAS_i(\lambda)\tau_i^{-1}} \qquad (18)$$

For a better illustration, the $DAS_i(\lambda)$ and corresponding spectral contours $F_{SS}{}^i$ of the two excited species of the Ba^{2+} complex are presented in Figure 6.

Although a calculation of the individual fluorescence quantum yields is impossible, it is reasonable to assume that the rate constants of fluorescence deactivation of the alkaline-earth metal ion complexes lie in the same range as those of the Mg^{2+} complex, **3**, **1**-H^+, and **2**-H^+, which are very similar (Table 3). The fluorescence decay times of the long-lived decay components of the Ca^{2+} and Sr^{2+} complexes are longer than that of the Mg^{2+} complex, pointing to higher fluorescence quantum yields of these species compared to that of the Mg^{2+} complex. Thus, the higher overall fluorescence quantum yield of the Mg^{2+} complex suggests the existence of a second weaker emitting conformer in the Ca^{2+} and Sr^{2+} complexes.

It is important to notice that, in contrast to the aforementioned, the determination of the complex stability constants is independent of the existence of differently emitting conformers as long as their absorption spectra do not differ and their concentration ratio remains constant during the titration. Since conformers are equilibrated, the latter assumption is always true; the former follows from the steady-state absorption and emission data. In this case the intensity of the emitted light is proportional to the total concentration and the determined complexation constants refer to the total complexation yielding the overall complex stability constant K_{tot}.

Although the exact molecular structure of the conformers remains obscure, the main conformational differences should reside at the nitrogen atom of the crown. The two conformers could differ in their twist angles between the phenyl ring and the BDP chromophore, which will vary their amount of CT interaction. As a second possibility, having the endo/exo isomerization of *N*-substituted aza crowns in mind, an equilibrium of a loose and a strong complex could affect both the pyramidalization and conformational flexibility at the nitrogen atom of the crown. Scheme 2 illustrates the different equilibria involved in complex formation of substituted aza crown ethers and metal ions in solution. Within this multistep Eigen−Winkler scheme, for a given aza crown ether the ratio of k_2/k_{-2} varies with the metal ion, counterion, and solvent, mainly depending on the thermodynamic parameters ΔS and ΔH for de/solvation of cation and crown, ion (pair) association, fit of cation into the cavity, and coordination of the cation to the crown's heteroatoms.[54,55] The influence of both reaction coordinates, pyramidalization, and conformational flexibility (e.g., twisting), on the LE and CT emission is well-documented for related donor−acceptor-substituted compounds and was intensively studied for alkylaminobenzonitriles. Nonetheless, the real mechanism is still not clear yet.[9d,46] We assume that both coordinates cannot be seen separately and depend on each other for the complexes studied here. As a direct consequence, electronic and conformational differences of the two conformers lead to differences in orbital overlap between the lone electron pair of the nitrogen atom and the aromatic π-system resulting in different CT quenching constants. Hence, different fluorescence decay times are observed for the LE emission.[56]

The stability constants measured for the cation complexes of **1** are in the order of $Ca^{2+} > Sr^{2+} > Ba^{2+} > Mg^{2+} > Li^+ > Na^+$, which can be explained by the cation size and the diameter of the crown moiety (Table 4) as well as the higher charge density of the divalent cations. Hence, divalent cations form more stable complexes compared to the monovalent ones. The value of the complexation constant *K* correlates well with the charge densities[57] n^2/r^{n+} as a measure for the electrostatic attraction in the complexes (ionic radii taken from ref 58). The exceptional behavior of the Mg^{2+} complex showing the highest FEF value, but only a moderate stability constant can be ascribed to the fact that the Mg^{2+} ion, which is too small to fit well into the cavity, has a strong affinity to the nitrogen donor atom of the crown. In contrast, the comparatively small Li^+ ion is

SCHEME 2: Generalized Kinetic Scheme for the Processes Participating in the Complex Formation of 1 and Metal Ion Perchlorates in Solution: Complex Formation of M^+ with a Substituted Aza Crown Ether Involving the Formation of a Contact Pair (Loose Complex, Step 1) and a (Strong) Complex (Step 2)

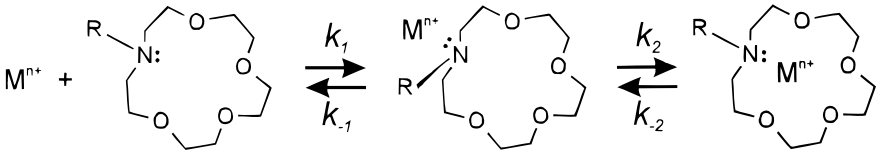

supposed to be coordinated mainly by the four crown oxygen atoms and one or two solvent molecules. This accounts for the much lower fluorescence enhancement because the inhibition of the nonradiative deactivation pathway can be only achieved by effective coordination of the metal ion to the crown nitrogen. The good correlation of FEF and n^2/r^{n+} for all the cations studied except for Li^+ confirms this complexation behavior. Similar effects have been found by us for intramolecular CT fluorescent probes as well.[59]

A closer examination of the fluorescence lifetimes of the complexes with Ca^{2+}, Sr^{2+}, Ba^{2+}, Li^+, and Na^+ reveals the following tendencies: (i) both fluorescence lifetimes increase with increasing values for FEF, and (ii) the increase in the relative amplitude of the fast component is in good correlation with the cation radius. The first correlation suggests that the increase in the fluorescence lifetimes of both components seems to be the direct consequence of the complex formation in the ground state and the emission of both excited complex conformers. Ca^{2+} forms the most stable complexes in the ground state, and they show the longest fluorescence lifetimes and highest fluorescence quantum yields. Assuming comparable rate constants of fluorescence deactivation for all the complexes studied,[60] the increase in τ_f and Φ_f suggest a decrease in k_{nr} with increasing complex stability.

On the other hand, the second correlation observed favors a predominantly sterically controlled mechanism being responsible for the ratio of the conformers formed. And indeed, the increase in the relative amplitude of the fast component with increasing cation radius suggests that the equilibrium of conformers in the ground state is mainly dependent on the size of the cation. The larger the cation complexed, the higher the relative amplitude of the weakly fluorescing conformer, the lowest relative amplitude being found in the case of Li^+.

Regarding the emission behavior of the complexes and the lack of a detectable CT emission, the excited complexes seem to be stable. No photoejection or decoordination of the cation could be observed. The complexes of **1** behave much more like PET probe complexes than typical ICT probe complexes, which leads to these analytically very valuable fluorescence enhancement factors.

Concluding Remarks

A comparison of the solvent-dependent absorption and emission properties of amino-substituted BDP dyes revealed that in a nonpolar solvent such as hexane emission occurs only from a LE state, whereas in more polar solvents an ultrafast excited-state charge-transfer reaction from the amino donor to the basic fluorophore takes place. This results in strong quenching of the LE emission and the appearance of a bathochromically shifted emission from a lower lying CT state, both fluorescence quantum yields being low. The efficient nonradiative deactivation process can be utilized to construct a very efficient molecular switch. Protonation as well as complexation blocks the CT process and switches on the LE emission again; i.e., a strong increase in LE fluorescence quantum yield and lifetime with very large fluorescence enhancement factors $>10^3$ results. Time-resolved measurements suggest that, with the exception of Mg^{2+}, all the complexes studied exist as two conformers in solution, which most likely differ in their conformation at the crown nitrogen.

The crowned BDP dye presented here is an example for a very efficient CT system that can be transferred to a LE system by stable cation complexation in polar acetonitrile. Thus, with dye **1**, we present a new design concept for extremely sensitive fluorescent probes for metal ions showing intense absorption and large fluorescence changes in an analytically useful wavelength region.

Acknowledgment. Financial support by the Deutsche Forschungsgemeinschaft (DFG), the Fonds der Chemischen Industrie, and the Bayerische Staatsregierung (Sonderprogramm für Infrastrukturmassnahmen) is gratefully acknowledged.

References and Notes

(1) Lakowicz, J. R. *Topics in Fluorescence Spectroscopy*; Plenum Press: New York, 1994; Vols. 1−4.

(2) Czarnik, A. W. *Fluorescent Chemosensors for Ion and Molecule Recognition*, ACS Symposium Series 538, American Chemical Society: Washington, D.C., 1993.

(3) Lockhart, J. C. Chemical sensors. In *Comprehensive Supramolecular Chemistry*; Lehn, J.-M., Ed.; Pergamon: New York, 1996; Vol. 1.

(4) (a) Fery-Forgues, S.; Le Bris, M. T.; Guetté, J. P.; Valeur, B. *J. Phys. Chem.* **1988**, *92*, 6233. (b) Bourson, J.; Valeur, B. *J. Phys. Chem.* **1989**, *93*, 3871. (c) Bourson, J.; Pouget, J.; Valeur, B. *J. Phys. Chem.* **1993**, *97*, 4552. (d) Martin, M. M.; Plaza, P.; Meyer, Y. H.; Badaoui, F.; Bourson, J.; Lefevre, J.-P.; Valeur, B. *J. Phys. Chem.* **1996**, *100*, 6879.

(5) (a) Jonker, S. A.; Ariese, F.; Verhoeven, J. W. *Recl. Trav. Chim. Pays-Bas* **1989**, *108*, 109. (b) Jonker, S. A.; van Dijk, S. I.; Goubitz, K.; Reiss, C. A.; Schuddeboom, W.; Verhoeven, J. W. *Mol. Cryst. Liq. Cryst.* **1990**, *183*, 273. (c) Jonker, S. A.; Verhoeven, J. W.; Reiss, C. A.; Goubitz, K.; Heijdenrijk, D. *Recl. Trav. Chim. Pays-Bas* **1990**, *109*, 154.

(6) Huston, M. E.; Haider, K. W.; Czarnik, A. W. *J. Am. Chem. Soc.* **1988**, *110*, 4460. Huston, M. E.; Engleman, C.; Czarnik, A. W. *J. Am. Chem. Soc.* **1990**, *112*, 7054. Czarnik, A. W. *Acc. Chem. Res.* **1994**, *27*, 302.

(7) Alfimov, M. V.; Gromov, S. P.; Lednev, I. K. *Chem. Phys. Lett.* **1991**, *185*, 455. Lednev, I. K.; Ye, T.-Q.; Hester, R. E.; Moore, J. N. *J. Phys. Chem. A* **1997**, *101*, 4966.

(8) Bissell, R. A.; de Silva, A. P.; Gunaratne, H. Q. N.; Lynch, P. L. M.; Maguire, G. E. M.; Sandanayake, K. R. A. S. *Chem. Soc. Rev.* **1992**, 187. de Silva, A. P.; Gunaratne, H. Q. N.; Kane, A. T. M.; Maguire, G. E. M. *Chem. Lett.* **1995**, 125.

(9) (a) Létard, J.-F.; Lapouyade, R.; Rettig, W. *Pure Appl. Chem.* **1993**, *65*, 1705. (b) Létard, J.-F.; Delmond, S.; Lapouyade, R.; Rettig, W. *Recl. Trav. Chim. Pays-Bas* **1995**, *114*, 517. (c) Mathevet, R.; Jonusauskas, G.; Rullière, C.; Létard, J.-F.; Lapouyade, R. *J. Phys. Chem.* **1995**, *99*, 15709. (d) Létard, J.-F.; Delmond, S.; Lapouyade, R.; Braun, D.; Rettig, W.; Kreissler, M. *Recl. Trav. Chim. Pays-Bas* **1995**, *114*, 517. (e) Cornelissen-Gude, C.; Rettig, W.; Lapouyade, R. *J. Phys. Chem. A* **1997**, *101*, 9673.

(10) Van den Bergh, V.; Meuwis, K.; Boens, N.; De Schryver, F. C.; Vincent, M.; Gallay, J.; Ameloot, M. *Proc. SPIE-Int. Soc. Opt. Eng.* **1994**, *2137*, 782. Meuwies, K.; Boens, N.; de Schryver, F. C.; Ameloot, M.; Gallay, J.; Vincent, M. *J. Phys. Chem. B* **1998**, *102*, 641.

(11) Fabbrizzi, L.; Poggi, A. *Chem. Soc. Rev.* **1995**, 197. De Santis, G.; Fabbrizzi, L.; Licchelli, M.; Sardone, N.; Velders, A. H. *Chem. Eur. J.* **1996**, *2*, 1243.

(12) Rurack, K.; Bricks, J. L.; Kachkovski, A. D.; Resch, U. *J. Fluoresc.* **1997**, *7*, 63S. Rurack, K.; Bricks, J. L.; Slominski, J. L.; Resch, U. *Dyes Pigm.* **1998**, *36*, 121.

(13) de Silva, A. P.; Gunaratne, H. Q. N.; Gunnlaugsson, T.; Huxley, A. J. M.; McCoy, C. P.; Rademacher, J. T.; Rice, T. E. *Chem. Rev.* **1997**, *97*, 1515 and references therein.

(14) Siemiarczuk, A.; Grabowski, Z. R.; Krowczinski, A.; Asher, M.; Ottolenghi, M. *Chem. Phys. Lett.* **1977**, *51*, 315.

(15) Siemiarczuk, A.; Ware, W. R. *J. Phys. Chem.* **1987**, *91*, 3677.

(16) Siemiarczuk, A.; Koput, J.; Pohorille, A. *Z. Naturforsch.* **1982**, *37a*, 598.

(17) Okada, T.; Mataga, N.; Baumann, W.; Siemiarczuk, A. *J. Phys. Chem.* **1987**, *91*, 4490.

(18) Mataga, N.; Nishikawa, S.; Asahi, T.; Okada, T. *J. Phys. Chem.* **1988**, *92*, 6233.

(19) Lee, S.; Arita, K.; Kajimoto, O.; Tamao, K. *J. Phys. Chem. A* **1997**, *101*, 5228.

(20) Wiessner, A.; Hüttmann, G.; Kühnle, W.; Staerk, H.*J. Phys. Chem.* **1995**, *99*, 14923.

(21) Herbich, J.; Kapturkiewicz, A. *Chem. Phys.* **1993**, *170*, 221.

(22) Onkelinx, A.; De Schryver, F. C.; Viaene, L.; van der Auweraer, M.; Iwai, K.; Yamamoto, M.; Ichikawa, M.; Masuhara, M.; Maus, M.; Rettig, W. *J. Am Chem. Soc.* **1996**, *118*, 2892.

(23) Herbich, J.; Kapturkiewicz, A. *J. Am Chem. Soc.* **1998**, *120*, 1014.

(24) Grabowski, Z. R.; Rotkiewicz, K.; Siemiarczuk, A.; Cowley, D. J.; Baumann, W. *Nouv. J. Chim.* **1979**, *3*, 443.

(25) Rettig, W. *Angew. Chem., Int. Ed. Engl.* **1986**, *25*, 971.

(26) Shiguza, H.; Ogiwara, T.; Kimura, E. *J. Phys. Chem.* **1985**, *89*, 4302.

(27) Plaza, P.; Dai Hung, N.; Martin, M. M.; Meyer, Y. H.; Vogel, M.; Rettig, W. *Chem. Phys.* **1992**, *168*, 365.

(28) Kollmannsberger, M.; Gareis, T.; Heinl, S.; Breu, J.; Daub, J. *Angew. Chem., Int. Ed. Engl.* **1997**, *36*, 1333.

(29) Gareis, T.; Huber, C.; Wolfbeis, O. S.; Daub, J. *Chem Commun.* **1997**, 1717.

(30) Werner, T.; Huber, C.; Heinl, S.; Kollmannsberger, M.; Daub, J.; Wolfbeis, O. S. *Fresenius J. Anal. Chem.* **1997**, *359*, 150.

(31) Molecular Probes Inc., Eugene, OR; URL: http://www.probes.com.

(32) Debreczeny, M. P.; Svec, W. A.; Wasielewski, M. R. *Science* **1996**, *274*, 584

(33) *Gmelins Handbuch der Anorganischen Chemie*, Chlor, 8th ed.; VCH: Berlin, 1927; p 402

(34) Olmsted, J., III. *J. Phys. Chem.* **1979**, *83*, 2581. Drake, J. M.; Lesiecki, M. L.; Camaioni, D. M. *Chem. Phys. Lett.* **1985**, *113*, 530.

(35) Resch, U.; Rurack, K. *Proc. SPIE-Int. Soc. Opt. Eng.* **1997**, *3105*, 96.

(36) Boens, N.; Tamai, N.; Yamazaki, I.; Yamazaki, T. *Photochem. Photobiol.* **1990**, *52*, 911.

(37) Eaton, D. F. *J. Photochem. Photobiol., B* **1988**, *2*, 523.

(38) Velapoldi, R. A.; Epstein, M. S. *ACS Symp. Ser.* **1989**, *383*, 98.

(39) Treibs, A.; Schulze L. *Liebigs Ann. Chem.* **1970**, *739*, 225.

(40) Dix, J. P.; Voegtle, F. *Chem. Ber.* **1980**, *113*, 457.

(41) de Wal, E. V.; Pardoen, J. A.; van Knoeveringe, J. A.; Lugtenburg, J. *Recl. Trav. Chim. Pays-Bas* **1977**, *96*, 306. Karolin, J.; Johansson, L. B.-A.; Strandberg, L.; Ny, T. *J. Am. Chem. Soc.* **1994**, *116*, 7801.

(42) Schütz, M.; Schmidt, R. *J. Phys. Chem.* **1996**, *100*, 2012.

(43) Rettig, W.; Maus, M.; Lapouyade, R. *Ber. Bunsen-Ges. Phys. Chem.* **1996**, *100*, 2091. Maus, M.; Rettig, W.; Lapouyade, R. *J. Inf. Rec.* **1996**, *22*, 451.

(44) Strehmel, B.; Seifert, H.; Rettig, W. *J. Phys. Chem. B* **1997**, *101*, 2232.

(45) Birks, J. B. *Photophysics of Aromatic Molecules*; Wiley: London, 1970.

(46) Schuddeboom, W.; Jonker, S. A.; Warman, J. M.; Leinhos, U.; Kühnle, W.; Zachariasse, K. A. *J. Phys. Chem.* **1992**, *96*, 10809. Leinhos, U.; Kühnle, W.; Zachariasse, K. A. *J. Phys. Chem.* **1991**, *95*, 2013.

(47) τ_0^{LE} and τ_0^{CT} are the fluorescence lifetimes of the LE and CT state, respectively. The calculation of the photophysical parameters is only possible if one of these fluorescence lifetimes is known. However, τ_0^{LE} can only be estimated from the fluorescence lifetime of a model compound that does not show the excited-state reaction investigated. Because of the independence on solvent polarity of the photophysical parameters k_f and k_{nr} of **3** and the similarity of these parameters for **1** and **2** in hexane, the value of τ_f of **3** in the corresponding solvent was chosen for τ_0^{LE}. Although in hexane, k_{nr} of **1** and **2** are somewhat larger than k_{nr} of **3**, which is most likely attributed to a low-lying nonpolar triplet state, the population of this state should be energetically unfavorable in the polar solvents diethyl ether and 1,4-dioxane. Thus, k_{nr} should decrease resulting in more similar values of k_{nr} for **1**, **2**, and **3** in the medium polar solvents, and τ_f of **3** is taken as τ_0^{LE}. However, the calculated values of k_{LC}, k_{CL}, and τ_0^{CT} show only minor changes (<5%) when choosing τ_f of **2** in hexane instead as value for τ_0^{LE}.

(48) Löfroth, J.-E. *J. Phys. Chem.* **1986**, *90*, 1160.

(49) Note that the value obtained by graphically analyzing this short wavelength part of the spectrum is in good agreement with the value of $Y = 5.11 \times 10^9\ s^{-1}$ obtained from a single set of amplitudes measured at the blue edge of the spectrum (cf. eq 6).

(50) The ratio c_{CT}/c_{LE} in eq 16 is a value obtained for photostationary conditions; i.e., for $c_{CT}/c_{LE}\ (t_{stat}) \geq 0.99 c_{CT}/c_{LE}\ (t_\infty)$. This equilibrium is reached after ca. 85ps in diethyl ether and 60ps in 1,4-dioxane, respectively.

(51) Svaan, M.; Parker, V. D. *Acta Chem. Scand. B* **1982**, *35*, 559.

(52) Piechowski, A. P. *J. Electroanal. Chem.* **1983**, *145*, 67.

(53) The small decrease in τ_f when going from 40:1 to 2250:1 is attributed to fluorescence quenching due to the heavy atom effect induced by the large excess of Ba^{2+} ions in the solution.

(54) Gokel, G. W.; Echegoyen, L.; Kim, M. S.; Eyring, E. M.; Petrucci, S. *Biophys. Chem.* **1987**, *26*, 225. Echegoyen, L.; Gokel, G. W.; Kim, M. S.; Eyring, E. M.; Petrucci, S. *J. Phys. Chem.* **1987**, *91*, 3854.

(55) Salomon, M.; Hefter, G. T. *Pure Appl. Chem.* **1993**, *65*, 1533. D'Aprano, A.; Salomon, M.; Mauro, V. *J. Solution Chem.* **1995**, *24*, 685.

(56) Note that the detection of any CT emission was not possible in acetonitrile.

(57) Here, the charge density is expressed as n^2/r^{n+}, the so-called "class A" or ionic index (cf. Nieboer, E.; Richardson D. H. S. *Environ. Pollut. Ser. B* **1980**, *1*, 3.).

(58) Shannon, R. D. *Acta Crystallogr.* **1976**, *A32*, 751.

(59) Rurack, K.; Bricks, J. L.; Resch-Genger, U. To be published.

(60) The values of k_f given in Tables 1 and 3 support the assumption that the rate constants of fluorescence deactivation of the complexes are comparable to those observed for **1**, **2**, and **3** under conditions when only the LE emission is present. The measured fluorescence lifetime and quantum yield, τ_f and Φ_f, and the radiative and nonradiative rate constants are linked by the following equations: $\tau_f = 1/(k_f + k_{nr})$ and $\Phi_f = k_f/(k_f + k_{nr})$. With $\Phi_f = k_f\tau_f$, not only the values obtained for F_{SS}^i from the time-resolved measurements (see eqs 10, 11, 18), but also the actual fluorescence quantum yields Φ_i of the complexes should increase with increasing complex stability.

(61) Measurements in chlorinated solvents were hampered by traces of HCl formed during the experiments. The much stronger fluorescence of the protonated species made the determination of spectral parameters of the free base impossible.

(62) Frensdorff H. K. *J. Am. Chem. Soc.* **1971**, *93*, 600. Dalley, N. K. In *Synthetic Multidentate Macrocyclic Compounds*; Izatt, R. M., Christensen, J. J., Eds.; Academic Press: New York, 1978; p 207.